ARMY RESEARCH LABORATORY

Electrospun Fibers for Composites Applications

by Joshua A. Orlicki, Joshua Steele, André A. Williams, George R. Martin, Eugene Napadensky, and B. Leighliter

ARL-TR-6800 **February 2014**

Approved for public release; distribution is unlimited.

NOTICES

Disclaimers

The findings in this report are not to be construed as an official Department of the Army position unless so designated by other authorized documents.

Citation of manufacturer's or trade names does not constitute an official endorsement or approval of the use thereof.

Destroy this report when it is no longer needed. Do not return it to the originator.

Army Research Laboratory
Aberdeen Proving Ground, MD 21005-5069

ARL-TR-6800 **February 2014**

Electrospun Fibers for Composites Applications

Joshua A. Orlicki and Eugene Napadensky
Weapons and Materials Research Directorate, ARL

Joshua Steele, André A. Williams, and B. Leighliter
Oak Ridge Institute for Science and Education

George R. Martin
Bowhead Science and Technology

Approved for public release; distribution is unlimited.

REPORT DOCUMENTATION PAGE	Form Approved OMB No. 0704-0188

Public reporting burden for this collection of information is estimated to average 1 hour per response, including the time for reviewing instructions, searching existing data sources, gathering and maintaining the data needed, and completing and reviewing the collection information. Send comments regarding this burden estimate or any other aspect of this collection of information, including suggestions for reducing the burden, to Department of Defense, Washington Headquarters Services, Directorate for Information Operations and Reports (0704-0188), 1215 Jefferson Davis Highway, Suite 1204, Arlington, VA 22202-4302. Respondents should be aware that notwithstanding any other provision of law, no person shall be subject to any penalty for failing to comply with a collection of information if it does not display a currently valid OMB control number.
PLEASE DO NOT RETURN YOUR FORM TO THE ABOVE ADDRESS.

1. REPORT DATE *(DD-MM-YYYY)*	2. REPORT TYPE	3. DATES COVERED (From - To)
February 2014	Final	1 October 2009–30 June 2013

4. TITLE AND SUBTITLE
Electrospun Fibers for Composites Applications

5a. CONTRACT NUMBER

5b. GRANT NUMBER

5c. PROGRAM ELEMENT NUMBER

6. AUTHOR(S)
Joshua A. Orlicki, Joshua Steele,[*] André A. Williams,[*] George R. Martin,[†] Eugene Napadensky, and B. Leighliter[*]

5d. PROJECT NUMBER

5e. TASK NUMBER

5f. WORK UNIT NUMBER

7. PERFORMING ORGANIZATION NAME(S) AND ADDRESS(ES)
U.S. Army Research Laboratory
ATTN: RDRL-WMM-G
Aberdeen Proving Ground, MD 21005-5069

8. PERFORMING ORGANIZATION REPORT NUMBER
ARL-TR-6800

9. SPONSORING/MONITORING AGENCY NAME(S) AND ADDRESS(ES)

10. SPONSOR/MONITOR'S ACRONYM(S)

11. SPONSOR/MONITOR'S REPORT NUMBER(S)

12. DISTRIBUTION/AVAILABILITY STATEMENT
Approved for public release; distribution is unlimited.

13. SUPPLEMENTARY NOTES
[*]Oak Ridge Institute for Science and Education, 4692 Millennium Drive, Suite 101, Belcamp, MD 21017
[†]Bowhead Science and Technology, 4900 Seminary Road, Suite 1200, Alexandria, VA 22311

14. ABSTRACT
A series of oriented electrospun nylon fibers were prepared with nominal fiber diameters of either 300 nm or 1 μm. In addition, a series of similar mats were prepared that contained a hyperbranched polymer additive to act as a surface modifier for the fibers. The mats were used as reinforcements for epoxy composites. The composite coupons were interrogated using techniques such as dynamic mechanical analysis and tensile testing. While the nanofibers did not dramatically stiffen the resulting composites, they provided insight as to the impact of the additives on the interaction of the fibers with the composite matrix. The inclusion of the additive appeared to improve interfacial interactions of the fibers with the matrix, as reduced void content and uniform fracture interfaces were observed in the modified composites. While the low production rate of suitable fiber mats for this study limited the scope and accessibility of test specimens, the results from the examination of fiber-matrix interfaces argues for further investigation.

15. SUBJECT TERMS
electrospinning, nanofiber, composite, hyperbranched polymer, SEM

16. SECURITY CLASSIFICATION OF:			17. LIMITATION OF ABSTRACT	18. NUMBER OF PAGES	19a. NAME OF RESPONSIBLE PERSON
a. REPORT	b. ABSTRACT	c. THIS PAGE			Joshua A. Orlicki
Unclassified	Unclassified	Unclassified	UU	38	19b. TELEPHONE NUMBER (*Include area code*) (410) 306-0931

Standard Form 298 (Rev. 8/98)
Prescribed by ANSI Std. Z39.18

Contents

List of Figures

List of Tables

Acknowledgments

The authors would like to thank Dr. Hong Dong for her assistance with the acquisition of scanning electron microscope micrographs of fiber composite fracture surfaces.

1. Introduction

Polymer-based composites represent a vast class of materials and, as a technology, impact everything from the automotive and construction fields to biotechnology. In recent years, one area of intense study has been the exploration of nanocomposites, where at least one of the dimensions of the filler component is below some threshold value, generally accepted to be ca. 100 nm. In some instances, nanocomposites have been shown to outperform analogous traditional (micro) composites by a wide margin. The keys to maintaining this performance benefit typically hinge upon limiting filler aggregation and ensuring positive filler-matrix interfacial interactions.

One approach to controlling nanofiller aggregation is to use preformed fillers, such as nanofibers, that are not capable of forming larger aggregates under processing conditions. While there are several approaches to generating nanofiber materials, perhaps the most widespread for laboratory work remains electrospinning, or e-spinning. The investigation of e-spun materials has exploded over the last 12+ years, and since the early reports (*1*), several research areas have received special attention. The fiber mat products of e-spinning are well suited for filtration, where tightly controlled fiber diameters, porosity, and low back pressure combine to provide filtration media with multifunctional capability. One recent report highlighted an e-spun nylon-6,6 mat combined with a polypropylene nonwoven mat to yield a hierarchically structured filter with high efficiency and low pressure drop (*2*). Another topic area of sustained interest is the exploration of fiber mats as substrates for the support of cellular growth. Fiber mat dimensions and alignment can be controlled and used to bias the growth of cells attached to the mats. This has been shown for a range of cells, including neuronal cells. In addition, the porosity of the fiber mats can be tuned to permit the infiltration of cells, providing three-dimensional substrates for cellular growth and a complimentary technology to hydrogel supports. Hierarchical structures can provide even greater flexibility in the fiber morphology accessible using this technique (*3*).

A third area of research concerns the use of nanofibers for composite reinforcement. The relationship between fiber diameter and polymer modulus has been explored by Rutledge and coworkers (*4*), who showed an increase in modulus as the fiber diameter was reduced. The rationalization for property improvement is based on the drawing of the fiber down to a nanoscale diameter (e.g., approaching ~300 nm and below), where polymer chain alignment and confinement (e.g., constrained conformation due to increased chain alignment) lead to enhanced strength. A similar trend has recently been reported for carbon fibers as well (*5*). Several groups have been exploring the use of nanofibers as reinforcement for polymer-fiber-based composites. There is considerable work exploring the use of e-spun fibers to form nanocomposites directly, where the spin-dope solution includes particulate fillers or reinforcements. The current study explicitly avoids this approach, although interested parties may find much information on these types of composites in the literature (*6*).

In one elegant example of composite research, investigators explored the use of core-shell-type fibers to reinforce acrylic-based resins (*7*). The shell of the reinforcing fiber was partially solvated or dissolved by the acrylic resin, which resulted in a very strong fiber-matrix bond. The materials exhibited a doubling of work of fracture in some cases, which was only observed when the core-shell reinforcement was present. Fibers of purely core material (with poor interfaces) or purely shell material (soluble) had little impact on the toughness of the composite. In addition to the core-shell-type fiber, several groups have explored the use of e-spun fibers as reinforcement for an epoxy matrix. One group explored the impact of fiber reinforcement of multiple fiber types on the physical properties of epoxy composites and found that polyurethane (PU) fibers increased the strain at break by more than a factor of 2. While the PU fibers did not dramatically strengthen the composite, other fibers (cellulose acetate) provided higher ultimate stress at the expense of strain (*8*). When nylons containing fibrillar silicate filler were used to reinforce a standard epoxy, increases in stiffness as well as toughness were observed (*9*).

Another area of current research for e-spun fiber mats is in their use to prepare hierarchically structured reinforcements for traditional composites. The motivation is that smaller fiber diameters will allow for greater interfacial interactions and reinforcement of interlayer areas in traditional woven mat composites. Nanofibrous interlayers were used to increase the impact and shear performance of a prepregged carbon fiber epoxy composite, with negligible impact on overall composite density or mass (*10*). A slightly earlier report also considered carbon fiber epoxy composites and demonstrated significant increases in both modes I and II fracture toughness (*11*). Additional studies expanding on the impact of nanofiber reinforcement of the interlaminar region may be found elsewhere (*12–16*). The use of discontinuous interleaves for damage control was also recently considered for modes I and II fracture and may be of benefit to interested readers (*17*).

The goal of this study was motivated along two themes by the above literature reports. First, we sought to compare the physical properties of composites reinforced with fiber mats of micro- and nanoscale fiber diameter on the expectation that the smaller mats would enable greater modulus gains using a standard engineering thermoplastic (nylon). The second goal of the study was to explore the impact of hyperbranched polymer (HBP) additives when included in the fiber spinning solution. The hypothesis was that the spontaneous surface enrichment that has been observed for these additives in earlier material matrices would be suitable to control surface composition of the fiber. This control would improve the fiber-matrix interface without requiring secondary processing techniques such as plasma treatment or fiber sizing to activate the fibers to enable thermodynamically favorable interactions with the epoxy resins.

2. Experimental Methods

2.1 Materials

Nylon-6,6 was obtained from Sigma Aldrich in pellet form and used as received. The preferred solvent for nylon dissolution was hexafluoro-isopropanol (HFiP), which was obtained from both Sigma Aldrich and Oakwood Chemicals.

A hyperbranched polyester (Boltorn H20) with an average molecular weight of 2000 Da was obtained from Perstorp Corporation. For purposes of stoichiometry determination, a repeat unit mass of 114.1 g/OH (hydroxyl group) was used, which neglected end group loss due to cyclization or the impact of polymer growth from a multifunctional core molecule. Hyperbranched polyethyleneimine (Lupasol g20wf) with an average molecular weight of 1300 Da, an amine ratio of primary (1°, terminal group):secondary (2°, linear segment):tertiary (3°, branch point) of 1.0:0.91:0.64, and an equivalent weight of 110 g/1° amine was obtained from BASF. Perfluorooctanoic acid was purchased from Exfluor Reseach Corporation. All other chemicals were purchased from Sigma-Aldrich or Alfa-Aesar and used as received.

2.2 E-Spinning Setup

Nylon was dissolved in HFiP to provide spin-dope solutions of varying concentrations. Nylon fibers were electrospun using a custom-built setup consisting of a syringe pump (Aladdin AL-1000) and a stationary aluminum plate (for randomly oriented fibers) or a rotating 1-in-diameter mandrel (for aligned fibers). The mandrel was connected to a motor (Dayton 115-V AC-DC) with a speed controller, allowing the mandrel to rotate between 0 and 8000 rpm. A 5-mL syringe was filled with polymer solution and fed through an 18-G stainless steel needle at flow rates of 1–5 mL/h with an applied potential of 18.5 kV. The gap between the needle and the collector was fixed at 7 in, and the collector was set to an applied potential of –3 kV. Fibers were maintained under ambient conditions for several hours and were stored in crystallization dishes, with individual mats wrapped in foil.

2.3 Additive Modification

A pair of HBPs was explored as potential additives to the nylon solutions. Hyperbranched polymers were obtained from commercial sources and modified using accepted methods. The hyperbranched polyethyleneimines (PEI) were amidated via an acid-catalyzed condensation reaction with a Dean Stark trap in refluxing toluene to drive conversion via the azeotropic removal of evolved water. The PEI (10 g, 90.9 mmol, 1° amine) was dissolved in 50-mL refluxing toluene, and lauric acid (0.2 eq. relative to 1° amine content, 18.2 mmol, 3.64 g) was added. After ca. 30 min., perfluorooctanoic acid (0.2 eq. relative to 1° amine content, 18.2 mmol, 7.53 g) was added, and the solution was allowed to react overnight. The product was dried via rotary evaporation without further purification. The modified HBPs were characterized with ^{1}H

and ^{13}C nuclear magnetic resonance spectrometry (NMR) and gel-permeation chromatography (GPC). The NMR analyses were carried out on a Bruker 600-MHz Avance spectrometer. Chemical shifts were referenced to the residual solvent peak ($CDCl_3$, 7.26 ppm for 1H, 77.36 for ^{13}C); integrations were based off of the methyl group of the aliphatic chain end for the ^1H spectra. ^1H NMR (600 MHz, $CDCl_3$) δ 8.11 (0.1 H), 7.20 (0.1 H), 7.12 (0.1 H, amide protons), 3.61 (0.3 H), 3.28, 3.22, 3.14, 3.08 (3.1 H, amide CH_2, PEI side), 2.75, 2.68, 2.62, 2.49 (42 H, backbone CH_2), 2.11 (2 H, aliphatic CH_2 α to amide), 1.55 (2 H, aliphatic CH_2 β to amide), 1.19 (17 H, aliphatic CH_2), 0.82 (3 H, aliphatic CH_3). ^{13}C NMR (151 MHz, $CDCl_3$) δ 181.19 (aliphatic CO), 161.95 (PFOA* CO), 129.26, 128.45, 125.52, 100.26 (CF_2, CF_3), 54.54, 52.44, 49.47, 47.61 (backbone CH_2), 41.64, 39.21 (CH_2 α to amide, PEI side), 36.87 (CH_2 α to amide, aliphatic side), 32.15, 29.88, 29.59, 27.10 (CH_2 aliphatic) 26.14 (aliphatic CH_2 β to amide, aliphatic side), 22.90 (CH_2 alpha to methyl group), 14.38 (aliphatic CH_3). Size measurements using triple-detector GPC were attempted, but there was insufficient refractive index signal in the tetrahydrofuran solvent; in toluene, the polymer appeared to be present solely as high-molecular-weight aggregates. Fourier-transform infrared spectroscopy analysis was also completed on the polymer, and the major peaks are listed in wave numbers (cm^{-1}): 3251 (H-bonding of amine), 2923, 2850 (aliphatic CH stretching), 1683, 1645, 1653 (carbonyl peaks), 1558, 1239, 1205, 1146.

Hyperbranched polyesters (PEs) were first modified using an adaptation of a known melt condensation procedure (*18*). The base PE-polyol (2.31 g, 20.3 mmol -OH) was melted at ca. 150 °C under a nitrogen purge and then combined with lauric acid (0.3 eq., 1.2 g) and perfluorooctanoic acid (0.2 eq., 1.70 g). A few milligrams of *p*-toluenesulfonic acid were added to catalyze the reaction. After homogenization, the melt temperature was raised to ca. 165° C for ca. 4 h under a constant flow of nitrogen. The solution was then allowed to cool to room temperature and dried under nitrogen. The resulting PE retained ca. 60% of the initial -OH groups and exhibited the form of a viscous oil with good solubility in common organic solvents.

The formation of PE-MAc was accomplished by taking the partially modified HBP into dichloromethane. To this solution was charged triethylamine (1.3 eq.), and the reaction vessel was purged with N_2 and chilled in an ice bath. To the cooled vessel was added methacryloyl chloride (1.2 eq.), dropwise, such that the temperature of the solution was maintained near the ice bath temperature. After the entire aliquot of methacryloyl chloride was added, the solution was stirred 30 min in the ice bath and was then allowed to slowly come to room temperature, where it was maintained for 3 days. The material was isolated by first removing solvent and any volatiles, followed by redissolution in dichloromethane. The organics were washed with water, sat. $NaHCO_3$, and brine in sequence, and then the organic layer was dried with Na_2SO_4. Drying the filtered product in vacuum yielded an off-white solid, which was stored in the freezer. HBPs were characterized with ^1H NMR. The NMR analyses were carried out on a Bruker 600-MHz

* PFOA = perfluorinated octanoic acid.

spectrometer. Chemical shifts were referenced to the residual solvent peak ($CDCl_3$, 7.26 ppm for ^1H reference). Integrations were based off of the aliphatic methyl group of the lauric acid. ^1H NMR (600 MHz, $CDCl_3$) δ 5.985 (2.4 H), 5.649 (2.1 H), 4.191 (10.9 H, backbone CH_2), 3.50 (5.7 H), 3.05 (1.5 H), 2.24 (1.3 H), 1.48 (1.3 H), 1.22 (21 H, aliphatic CH_2, and backbone CH_3), 0.84 (3 H, aliphatic CH_3). Further characterization was complicated by the poor diminishing solubility of the PE-MAc structure over time; the high local density of methacrylate groups led to a low threshold for cross-linking of the HBP. This route was abandoned after initial synthesis and studies. Addition of radical scavengers to the purified product might have improved stability, but this procedural modification was not pursued.

2.4 Surface Characterization

X-ray photoelectron spectroscopy (XPS) data was obtained using a Kratos Axis Ultra X-ray photoelectron spectroscopy system, equipped with a hemispherical analyzer. A 100-W monochromatic Al Kα (1486.7 eV) beam irradiated a 0.5- × 1.0-mm sampling area. Survey scans were taken at pass energy = 80 eV. Elemental high-resolution scans for C 1*s*, O 1*s*, N 1*s*, Cl 2*p*,and F 1*s* were taken at pass energy = 20 eV. CasaXPS software was used for all data analysis. In instances where Si was detected, it was attributed to SiO_2 contamination or pinholes in the film, so the Si value was disregarded and the corresponding oxygen signal was corrected by an appropriate amount (e.g., reduced O 1*s* signal by twice the Si measured); the quantification values presented in the following sections were normalized to 100% using this correction factor.

Scanning electron micrographs were obtained using a Hitachi S-4700 scanning electron microscope (SEM) at an accelerating voltage of 5 kV. The samples were sputter-coated to reduce charging before SEM operation.

2.5 Composite Preparation (Layup)

Several matrices and layup procedures were explored to enable the incorporation of nanofiber mats into epoxy-based resin systems. Initial studies employed SC-15 resin (from Applied Poleramic, Inc.) for dynamic mechanical analysis (DMA) experiments, and vacuum-assisted transfer molding (VARTM) was evaluated. The flow of resin in the VARTM process led to localized disruption of the fiber mats (e.g., bunching of fibers), reducing the yield of the final part. The resin, a toughened two-phase epoxy, proved somewhat difficult to analyze, so a simpler, untoughened epoxy system was sought.

Tensile specimens were explored using Epon 825 from Momentive and later formulations employed bisphenol A diglycidyl ether (DGEBA) combined with jeffamine D230 (a polyamine). Composite generation followed a wet layup procedure, where the fully mixed resin system was poured to completely cover each nanofiber mat as each mat layer was laid upon another. After being bagged with other scheduling and placed under vaccum, excess resin was drawn out of the part as the composite system was cured at 80 °C overnight (16 h) and then postcured at 120 °C for 1 h.

2.6 Composite Characterization

Composites were characterized using DMA. A large rectangular sample was made as a composite billet, and DMA samples with a specific geometry of 35 × 12 × 2.6 mm were cut from the larger part. Further surface preparation was required to ensure samples were within 0.07 mm of set requirements by manually sanding to reduce surface imperfections created by the molding process. Samples were tested with a Q800 TA DMA in a 35-mm short dual cantilever clamp system with sinusoidally applied oscillatory stresses (12-μm amplitude, 1-Hz fixed frequency) and analyzed in a temperature range of 25 to 150 °C.

Test coupons for tensile experiments were prepared by using the wet layup procedure to form a large composite film/plate, and then a water-jet cutter was programmed to form dog-bone geometries from the composite plate. The dog-bone samples were then measured for gage length and cross section using a pair of calipers, and the samples were tested using an Instron 5500R1123 with a 5-kN load cell.

3. Additive Modification Approaches

A small library of spontaneously segregating additives was targeted for incorporation into the nylon solutions. The primary goal of additive incorporation was to modify fiber surface characteristics without employing secondary processes such as plasma activation or silane treatement. These additives were based on the Macromolecular Transport Vehicle developed at the U.S. Army Research Laboratory (*19*). These materials are based on commercially available HBP scaffolds with primary amine (BASF Lupasol g20wf) or primary alcohol (Perstorp Boltorn H20) chain ends.

The Lupasol-based material was functionalized with both lauric and PFOA chain ends via an amidation driven by azeotropic removal of water from a toluene reaction solution, as shown in figure 1. This polymer was modified based on the stoichiometry of primary (1°) amine chain ends, with ca. 20% converted to amides for each lauric and PFOA amide. The resulting material, identified simply as PEI, retained ca. 60% of the 1° chain ends, as well as the secondary (2°) amines along the linear section of the polymer backbone. No additional modification was necessary to provide this additive with moieties reactive toward composite resin chemistry; amines may react directly with the epoxy group found in epoxy resins and may also react through Michael addition reaction with acrylates and methacrylates found in vinyl ester resin systems.

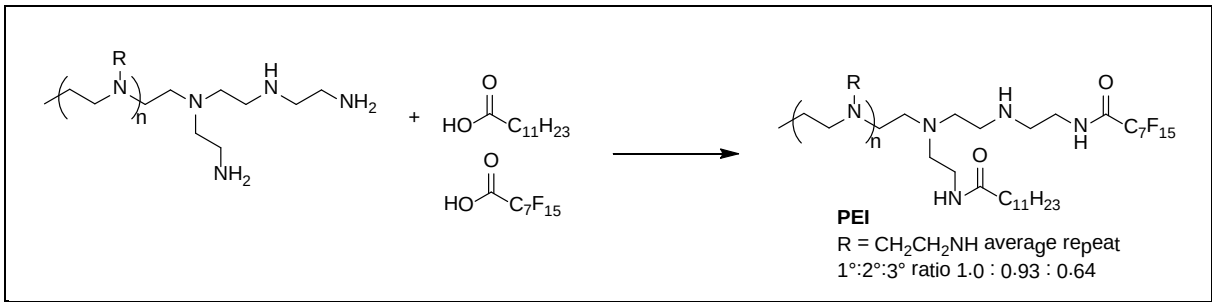

Figure 1. Functionalization of polyethyleneimine to form PEI.

The Perstorp Boltorn materials were functionalized similarly, with both lauric and PFOA chain ends, as shown in figure 2. The remaining chain ends were all primary alcohols, so they required additional modification to be reactive in the intended resin systems. The chain ends were functionalized using methacryloyl chloride to install methacrylate esters onto the HBP periphery. These groups would be active in a vinyl ester resin system through the standard free-radical cure mechanism and could react with the amines in an epoxy-amine system via Michael addition reactions. The methacrylated polyester is identified as PE-MAc. Some additional synthetic targets were pursued initially but were later abandoned because of synthetic difficulties and low probability of success. These targets and a brief discussion of their synthesis appear in the appendix.

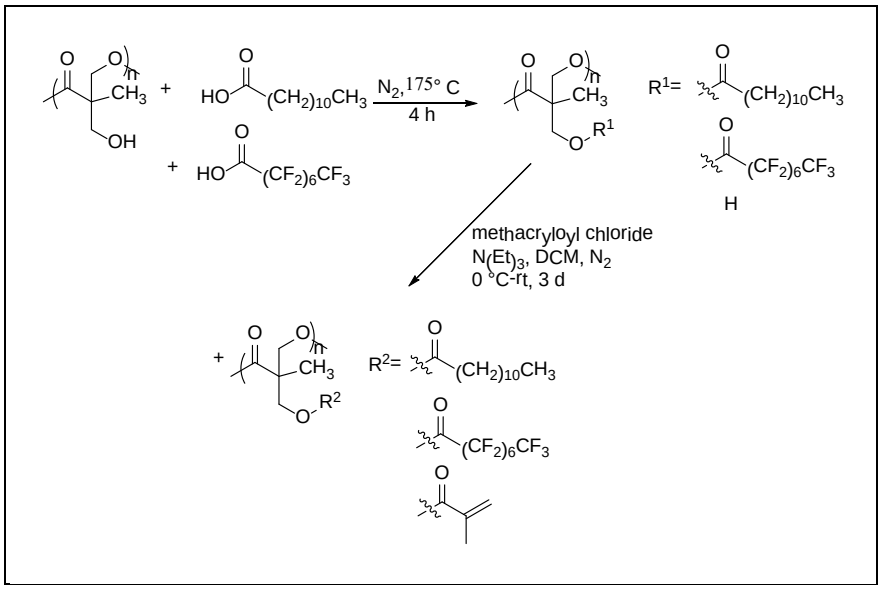

Figure 2. Functionalization of polyester to form PE-MAc.

4. Fiber Preparation and Characterization

Initial experiments with the electrospinning apparatus concerned the establishment of spinning conditions correlated to resultant fiber properties. Process variables, including polymer concentration, cosolvent composition, applied voltage, target voltage, flow rate, and salt inclusion, were all examined. The desired fiber characteristics were centered on diameter, and mean values of ca. 1 μm and 300 nm were nominally targeted. This bracketing was intended to demonstrate the value, if any, of decreasing fiber diameter for composite reinforcement. Fiber diameter was determined by surveying fiber mats with scanning electron microscopy; stated values are an average of at least 20 measurements of individual fiber diameters. A summary of process conditions and resulting fiber diameters is provided in table 1. Images of fibers representing the preferred conditions are shown in figure 3.

Table 1. Fiber diameter as a function of process conditions.

Sample No.	Substrate Concentration	Time (h)	Flow Rate (mL/h)	Bias (kV)	Mandrel Speed	Humidity (%)	Film Thickness (mil)	Fiber Thickness (µm)
BJ-01	10% Nylon 6,6 5% DMF	2	3	+18 –3	4.5	27	9.707	—
BJ-02	10% Nylon 6,6 5% DMF	2	3	+20 –3	4.5	30	4.799	1.273
BJ-03	10% Nylon 6,6 5% DMF	2	2	+18 –3	4.5	32	—	1.352
BJ-04	5% Nylon 6,6 5% DMF	2	3	+18 –3	4.5	32	1.759	0.476
BJ-05	2% Nylon 6,6 5% DMF	2	3	+18 –3	4.5	20	1.521	0.15
BJ-06	12% Nylon 6,6 5% DMF	2	3	+18 –3	4.5	36	—	13.600
BJ-07	8% Nylon 6,6 5% DMF	2	3	+18 –3	4.5	34	—	1.536
BJ-08	8% Nylon 6,6 5% DMF	3	2	+18 –3	4.5	41	2.325	0.929
BJ-09	12% Nylon 6,6 5% DMF	3	2	+18 –3	4.5	40	5.807	1.605
BJ-10	8% Nylon 6,6 5% DMF	3	3	+18 –3	4.5	38	0.685	1.106
BJ-11	12% Nylon 6,6 5% DMF	2	2.5	+15 –3	4.5	30	2.845	1.915
BJ-12	7% Nylon 6,6 5% DMF	3	2.5	+15 –3	4.5	28	8.663	0.728
BJ-13	14% Nylon 6,6 5% DMF	3	2	+15 –3	4.5	38	8.680	5–10 melt
BJ-14	9% Nylon 6,6 5% DMF	3	2	+15 –3	4.5	38	14.047	1.288
BJ-15	4% Nylon 6,6 5% DMF	3	2.5	+15 –3	4.5	23	4.537	0.292
BJ-16	3% Nylon 6,6 5% DMF	3	2.5	+15 –3	4.5	36	3.234	0.243
BJ-17	11% Nylon 6,6 5% DMF	3	2.5	+15 –3	4.5	36	0.796	1.769
BJ-18	5% Nylon 6,6 5% DMF	3	2.5	+15 –3	4.5	21	3.593	
BJ-19	8% Nylon 6,6 5% DMF	3	2.5	+15 –3	4.5	20	9.927	0.891
BJ-20	9% Nylon 6,6 5% DMF 5% Water	3	2.5	+15 –3	4.5	21	16.205	1.115
BJ-21	9% Nylon 6,6 5% DMF	3	2.5	+15 –3	4.5	21	3.897	1.243
BJ-22	10% Nylon 6,6 5% DMF 5% Water(+0.5%LiCl)	3	2.5	+15 –3	4.5	23	7.945	2.902 6.779
BJ-23	10% Nylon 6,6 5% DMF 5% Water(+0.5%LiCl)	3	2.5	+15 –3	4.5	23	—	
BJ-24	10% Nylon 6,6 5% DMF(+0.5%LiCl)	3	2.5	+15 –3	4.5	23	8.947	5–10 melt additive
BJ-25	10% Nylon 6,6 5% DMF(+0.5%LiCl)	3	1-3	+15+18 –3	4.5	24	—	5.923
BJ-26	10% Nylon 6,6 5% DMF 0.25% PEI	3	2.5	+15 –3	4.5	22	15.893	1.548
BJ-27	10% Nylon 6,6 5% DMF 0.34% PEI	4	2.5	+15 –3	4.5	22	27.907	1.786
BJ-28	10% Nylon 6,6 5% DMF 5% Water(+0.5%LiCl)	4	2.5	+15 –3	4.5	24	14.04	2.465
BM-38	10% Nylon 6,6 5% DMF	3	2	+15 –3	4.5	37	—	1.381
BM-39	10% Nylon 6,6 5% DMF 0.1% PEI	3	2	+15 –3	4.5	44	—	1.538
BM-44	10% Nylon 6,6 5% DMF 0.1% AAW-3-162 meth.	1.75	2.2	+15 –3	4.5	32	—	0.919 7.824
BJ-29	6% Nylon 6,6 5% DMF		1.2	+15 –3	4.5	LO	—	0.965

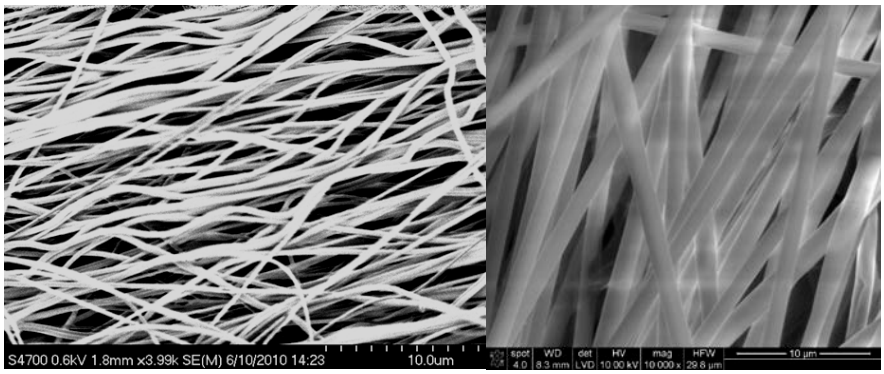

Figure 3. Representative images of nylon 6,6 fibers, ca. 300 nm (left) and ca. 1 mm (right).

In addition to the study of nylon-6,6 fibers, the fiber morphology of blended materials was also studied. We examined the incorporation of either the PEI or base PE (lacking the MAc groups) additive. The PEI was explored up to 10% loading based on total system solids, while the base PE was explored at loadings up to only 1%. In both instances, the inclusion of the additives did not substantially change the observed fiber diameters achieved through the e-spinning process; representative dimensions of fiber mats incorporating 1% additive are shown in figure 4. The inclusion of unmodified PEI (e.g., retained unmodified amine chain ends and backbone units) has been reported previously in an e-spun fiber system with polyamide-6, although in that instance a high-molecular-weight PEI (70 kDa) was spun on top of the polyamide mat to yield a sensing component on a quartz crystal microbalance substrate (*20*).

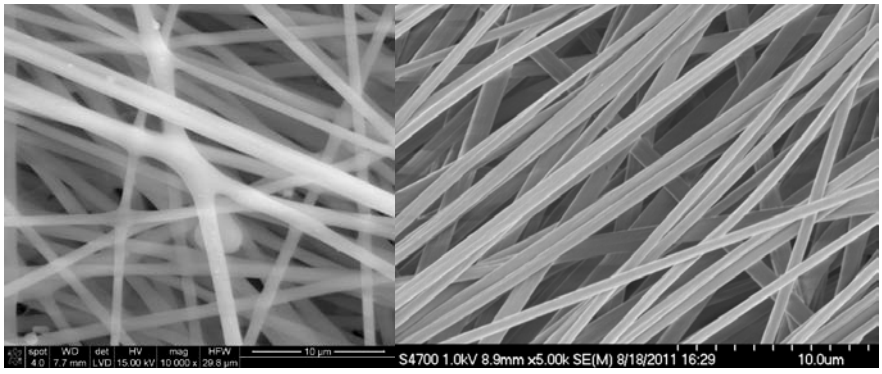

Figure 4. Fiber dimensions were maintained with addition of 1% PE-MAc (left) or 1% PEI (right).

The surface composition of the fibers was analyzed using XPS. This technique provides the elemental composition (note that protons not observed) of the top ca. 10 nm of a surface, although angle-resolved techniques may decrease the depth of analysis. For the current study, the detector was maintained normal to the fiber mat surface, so the depth of analysis was at the maximum value. The quantitative results are provided in table 2, and representative plots of the survey scans are provided for two samples in figure 5. The baseline nylon-6,6 fibers exhibited C, N, and O at the fiber surface, as anticipated. The lack of the F signal was also anticipated and indicates that the solvent used for fiber spinning, HFiP, was fully removed from the surface of the fibers. The PEI additive was evaluated at multiple loadings, while the PE-MAc was considered at just 1% loading. The loadings are expressed as a fraction of total solids mass for each formulation.

Table 2. Surface composition of e-spun fibers.

Sample	% C		% O		% N		%F	
Commercial nylon	78.7	+/– 0.6	11	+/– 1	10.3	+/– 0.6	—	—
E-spun nylon	82.7	+/– 1.2	9	+/– 0.1	8.7	+/– 0.6	—	—
ES-nylon, PE-MAc	81.7	+/– 0.6	8.3	+/– 0.6	10	+/– 0.1	—	—
ES-nylon, 1% PEI	79.8	+/– 0.6	8.8	+/– 0.3	10.7	+/– 0.3	0.7	+/– 0.1
ES-nylon, 10% PEI	76.7	+/– 0.6	8	+/– 0.1	9.7	+/– 0.6	5.5	+/– 0.9
ES-nylon, 40% PEI	71.7	+/– 1.5	6	+/– 0.1	12	+/– 0.1	10.3	+/– 0.6

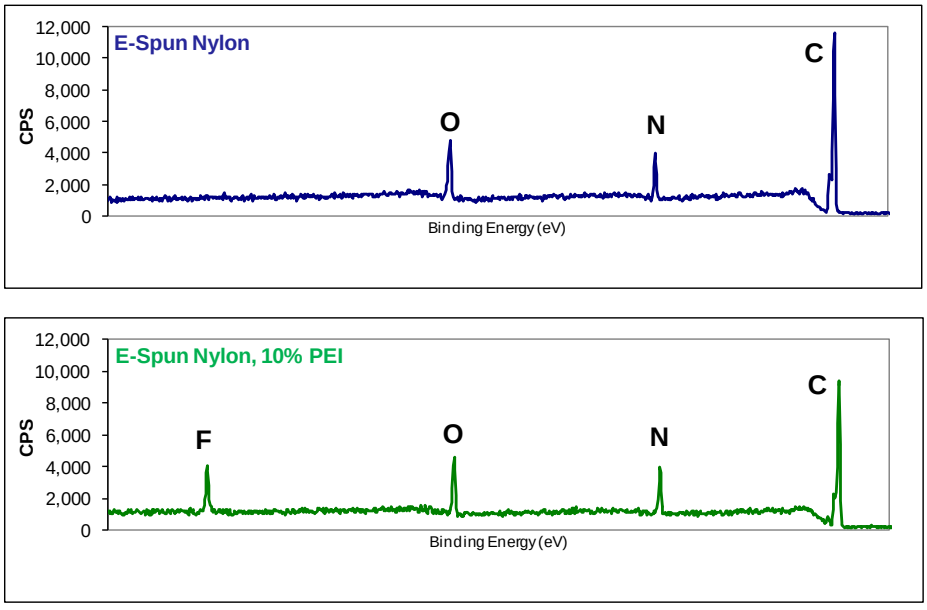

Figure 5. XPS survey scans quantifying elemental composition. (Note the strong F signal observed in the modified fiber mat [lower], indicative of high additive content at the fiber surface.)

The results of the XPS are consistent with the modification of the fiber surface by the PEI, but there is little evidence that the PE-MAc was present at the fiber surface. Values of fluorine and nitrogen at the fiber mat surface for the samples containing PEI were somewhat lower than those observed previously for e-spun systems in poly(methylmethacrylate) (PMMA) (*21*). It is hypothesized that the solvent used to enable the spinning of nylon-6,6, HFiP, reduced the effectiveness of the perfluorinated "buoy" groups on both the PE-MAc and PEI additives. In most film or fiber applications, these additives are driven to the air interface by surface energy mismatch with the surroundings, driven primarily by their perfluorooctanoic and aliphatic chain ends. In a highly fluorinated solvent, however, the compatibility between the chain ends and the solvent is improved; this improvement likely resulted in the lower migration efficiency shown here. The observed F signal for the PEI additive, however, suggests that the additive has migrated to the fiber surface during the spinning and drying process and that the route for surface modification remained viable.

Fiber mats for composite applications were prepared using the 3% (comparable to BJ-15) and 8% (comparable to BJ-19) solutions indicated in table 1. The fibers obtained under these conditions were nominally 300 nm and 1 μm, respectively. The mats were collected on a rotating mandrel but could be removed from the substrate and lain flat. The mats were approximately 3 × 6 inches in size, which determined the maximum size of the composite that could be prepared.

5. Composite Preparation and Characterization: DMA

Composites were initially prepared using the SC-15 toughened resin system from Applied Poleramics, Inc. Composite generation followed a wet layup procedure, where the fully mixed resin system was poured to completely wet and cover each nanofiber mat, as successive mats were laid upon the preceding layer. After being bagged with appropriate release and bleeder plies, the composite assembly was placed under vacuum, excess resin was forced out of the part, and the system was cured at 80 °C overnight (16 h) and then postcured at 120 °C for 1 h. Composite specimens with eight plies of fiber were evaluated using DMA, as was a sample containing commercial fabric fibers (note the fabric was a 0°/90° weave). Freeze fracture interfaces of two of the DMA specimens are shown in figure 6, which highlights the size difference between the commercial and e-spun fibers. The e-spun fibers also demonstrated less void volume around the fibers, indicating reasonably good interfaces.

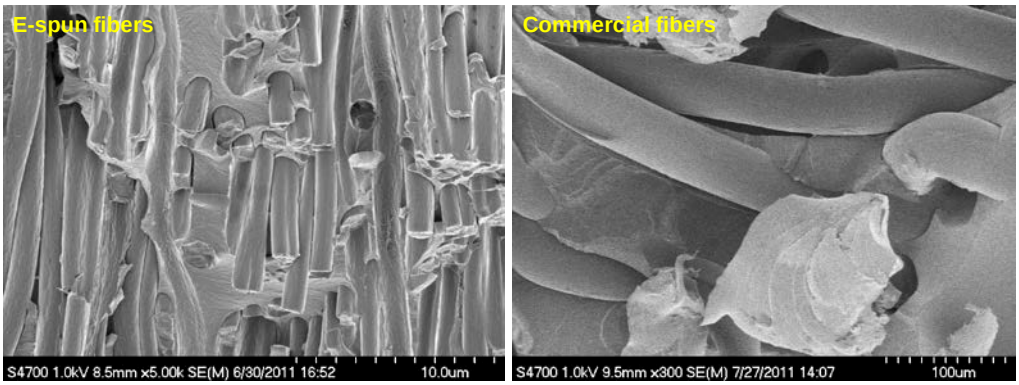

Figure 6. Freeze-fractured surfaces of e-spun (left) and commercial (right) nylon fibers in epoxy matrix. Note the difference in scale bars for each image.

The DMA experiment consisted of subjecting the test specimen to an oscillatory load (1 N) as the temperature was gradually increased. The changeover from the stiff glassy region to the rubbery region is governed by the epoxy glass transition temperature and characterized by a change in storage modulus of at least an order of magnitude. The plot in figure 7 shows that the inclusion of the fiber reinforcement reduced the modulus in the glassy region but actually stiffened the composite in the rubbery region. The change in storage modulus for the reinforced sample is markedly less than the change demonstrated by the unfilled epoxy resin. Similar performance was observed when commercial fibers were compared with the e-spun fibers for reinforcement. The commercial fibers improved the storage modulus in the rubbery plateau relative to the baseline epoxy, but the net improvement was smaller in magnitude than the composites reinforced by the e-spun fiber mats.

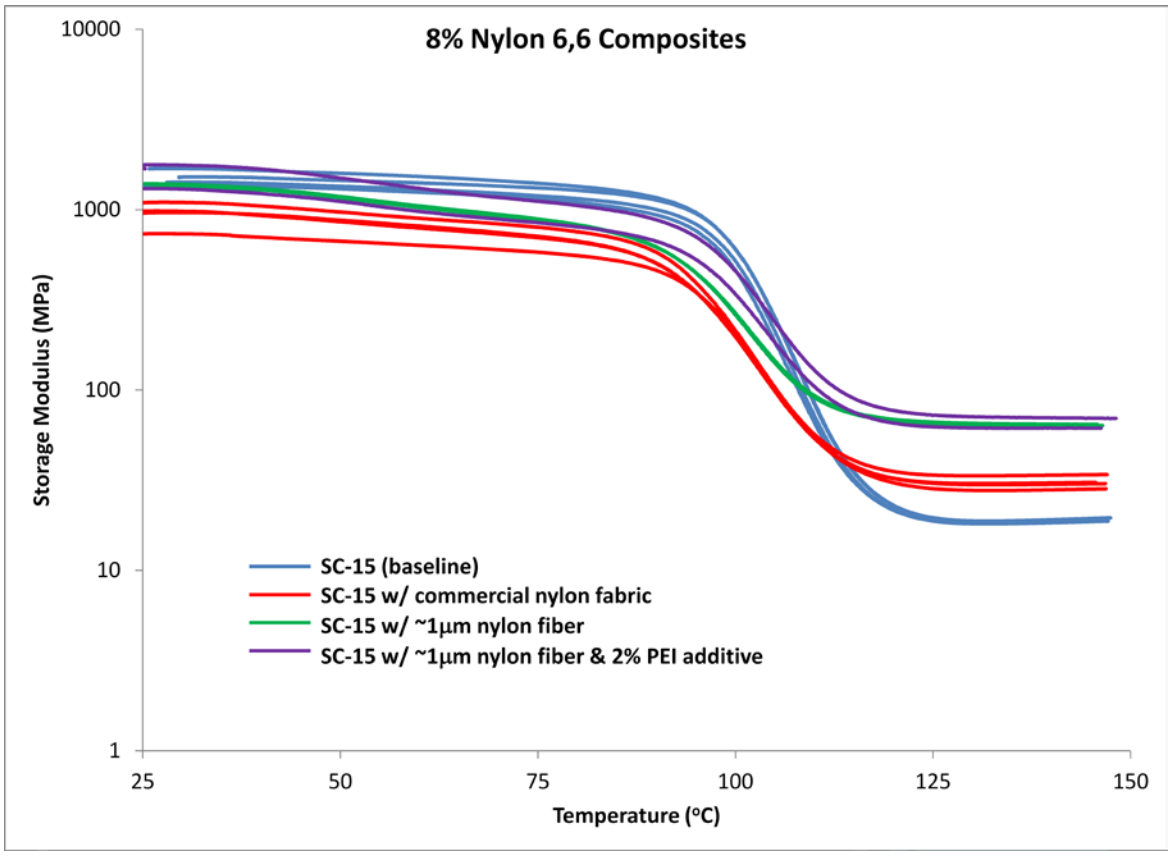

Figure 7. DMA of epoxy fibers exploring impact of fiber diameter and additive content on composite characteristics. Note the changes in the rubbery plateau region, where e-spun fibers strengthen more than commercial fabric, which is better than neat resin.

6. Composite Preparation and Characterization: Tensile Strength Analysis

Tensile specimens were prepared using a simplified epoxy formulation employing DGEBA combined with jeffamine D230 (a polyamine). Composite generation followed the same procedure described previously. Nylon fibers were spun at 3% loading to yield fibers with nominal 300-nm-diameter thickness, while 8% loading was employed to provide fiber diameters of ca. 1 µm.

We determined the composite density using Archimedes principle (table 3), enabled by a balance equipped with both a standard-weighing pan as well as a weighing cradle suspended in a liquid of known density (water, $\rho = 0.997$ at laboratory conditions). The total mass of fiber incorporated into each composite (m*f*) and the total mass of the composite (m*c*) allowed the calculation of the mass of the matrix (m*m*) by difference analysis (table 4). Combined with the

baseline densities of the nylon-6,6 and resin matrix, this information allowed us to estimate fiber volume fraction (V_f table 4). While there was some variability in the experimental samples, they all resided in a range from 10% to 20% volume fraction, except for the commercially sourced fiber, which was substantially higher.

Table 3. Density determination of composite specimens.

Sample Name	Dry Weight (g)	Buoyant Weight (g)	ρ Composite (g/mL)
300-nm nylon6,6_PEI_E825/D230	0.5335	0.0659	1.14
300-nm nylon6,6_E825/D230	0.6175	0.0567	1.10
1-mm nylon6,6_PEI_E825/D230	0.3276	0.0408	1.14
1-mm nylon6,6_E825/D230	0.4498	0.0578	1.14
Commercial nylon	0.0783	0.0024	1.03

Table 4. Fiber volume fraction determination of composite specimens.

Sample Name	Volume Fiber Fraction				
	m_f	m_c	m_m	W_m	V_f
300-nm nylon6,6_PEI_E825/D230	1.540	13.560	12.020	88.64	0.128
300-nm nylon6,6_E825/D230	1.494	10.588	9.094	85.89	0.184
1-mm nylon6,6_PEI_E825/D230	1.749	11.040	9.291	84.16	0.171
1-mm nylon6,6_E825/D230	1.723	7.482	5.759	76.97	0.238
Commercial nylon	1.769	3.060	1.291	42.19	0.625

To study the impact of the fiber reinforcement, the composite plaques were cut into tensile test specimens (i.e., dog-bone geometry) using a water-jet cutter. The tensile properties of the composite were determined using a crosshead speed of 1 mm/s and a 5-kN load cell. Strain was determined using digital image correlation (DIC), facilitated by a speckled pattern painted on each specimen; DIC provided strain measurements free of mechanical correction factors.

Results of the tensile testing are presented in table 5, which identifies peak stress and strain for each sample, stress and strain at failure, and modulus derived from the low-strain portion of the stress-strain curve. Several of the samples exhibited anomalous behavior when plotted as stress-strain curves, all of which are provided in the appendix. The plots are presented with common axes for the neat epoxy and e-spun fiber–containing samples. The commercial fiber composites exhibited much higher stress and strain, which required extended axes to fully encompass the data. The improved performance of the commercial material was likely enabled by the 0°/90° weave of the fiber, which was unique amongst the reinforcements tested here. All of the e-spun fibers were aligned nominally along the axis of the tensile strain, so no lateral reinforcement was incorporated into the composite structure.

Table 5. Tensile test results of e-spun fiber composites.

Sample Name	Sample No.	Testing Dimensions (mm)			X Area (mm^2)	Peak Stress	Peak Strain	Stress at Failure	Strain at Failure	Stiffness	Stiffness Averaged
		Gage L	Width	Thickness							
300-nm Nylon6,6_PEI_E825/D230	3PEI1	—	4.14	2.01	8.3214	23.73	0.02	23.69	0.02	1651.57	2354
Vf	3PEI2	—	4.06	1.33	5.3998	—	—	—	—	—	—
0.1279	3PEI3	—	4.12	2.1	8.652	40.74	0.02	40.44	0.02	2696.52	2706
—	3PEI4	—	4.05	1.5	6.075	42.55	0.02	42.31	0.02	2714.72	—
300-nm Nylon6,6_E825/D230	3NO1	—	4.51	1.97	8.8847	40.25	0.02	30.54	0.04	2391.03	2595
Vf	3NO2	—	4.43	1.44	6.3792	45.85	0.02	44.91	0.02	2836.14	—
0.1845	3NO3	—	4.37	1.38	6.0306	43.86	0.02	43.86	0.02	2587.57	—
—	3NO4	—	4.38	1.31	5.7378	35.79	0.01	35.79	0.01	2563.42	—
1-mm Nylon6,6_PEI_E825/D230	8PEI1	—	4.45	1.59	7.0755	49.16	0.03	43.64	0.03	3135.90	2910
Vf	8PEI2	—	4.45	1.51	6.7195	49.86	0.03	47.64	0.05	2665.88	—
0.1711	8PEI3	—	4.42	1.05	4.641	52.77	0.04	52.05	0.04	2927.17	—
—	8PEI4	—	4.41	1.15	5.0715	—	—	—	—	—	—
—	8PEI5	—	4.43	0.46	2.0378	—	—	—	—	—	—
1-mm Nylon6,6_E825/D230	8NO1	—	4.08	0.87	3.5496	51.20	0.04	50.09	0.05	2863.10	2725
Vf	8NO2	—	4	0.55	2.2	41.20	0.02	41.07	0.03	2356.85	—
0.2384	8NO3	—	4.25	1.73	7.3525	46.51	0.02	46.19	0.02	2953.77	—
Commercial nylon	1COMM	—	4.21	0.3	1.263	85.83	0.24	85.83	0.24	2020.29	1930
Vf	2COMM	—	4.26	0.3	1.278	83.45	0.24	81.85	0.24	1864.15	—
0.6247	3COMM	—	4.28	0.3	1.284	86.99	0.25	85.05	0.26	1904.14	—
Neat no post	Neat1	—	4.13	2.16	8.9208	—	—	—	—	—	—
Vf	Neat2	—	4.14	2.18	9.0252	53.82	0.03	52.16	0.04	2924.92	2902
0	Neat3	—	4.12	2.29	9.4348	55.95	0.04	50.55	0.06	2878.69	—
—	Neat4	—	4.13	2.32	9.5816	55.32	0.04	49.06	0.07	2903.34	—
Neat post	2Neat1	—	4.05	2.25	9.1125	57.20	0.04	51.48	0.05	3536.25	3194
Vf	2Neat2		4.35	2.28	9.918	57.37	0.03	42.14	0.06	2852.21	—
0	—	—	—	—	—	—	—	—	—	—	—

The observed stiffness of the composites was uniformly lower than that observed for the neat resin samples. The resin was a mixture of Epon 825 as the epoxy component and Jeffamine 250 as the amine component. Without a postcure, the resin system exhibited a modulus of 2.9 GPa; a slightly higher modulus (3.1 GPa) was obtained through the use of a postcure thermal treatment.

$$\sigma_{comp} = \sigma_1 V_{f1} + \sigma_2 V_{f2} + \sigma_3 V_{f3} + \ldots \quad (1)$$

The inclusion of nylon-6,6 fibers universally weakened the epoxy, even when measured along the axis of the fiber. The first series of data shown in table 5 is for the smallest-diameter fibers with the PEI additive; three samples were prepared successfully, and, curiously, two of them grouped closely in materials performance while the third diverged substantially. The performance of a composite in tension with aligned fibers can most simply be described by the addition of moduli of the constituent materials based upon their contribution to the whole composite based on volume fraction (equation 1). Using this approximation, we calculated an effective modulus for the nylon reinforcement. These values ranged from negative values in one instance to between 1.2 and 2.9 GPa (Stiffness Averaged column in table 5). This spread encompasses the modulus accepted for bulk nylon and indicates the potential for improved properties as a function of draw ratio. The selection of a high-modulus epoxy, while relevant to Department of Defense applications, complicated the analysis of the fiber impact due to the high modulus of the baseline material.

The impact of the additive on the nylon fibers and the resultant interface with the epoxy matrix is similarly difficult to deconvolute. In the case of the 1-μm fibers, the fibers produced with the PEI additive exhibited higher modulus than the comparable composite that lacked the PEI additive. Consideration of the 300-nm fiber composites flips the results, where the baseline nylon fibers outperformed the PEI-modified material. The reduced modulus of the PEI-nylon composite disappears if the "outlier" tensile specimen is dropped from the analysis, and then the trend matches the behavior of the larger fibers. The small number of replicates tested for each composition renders any conclusions drawn about performance impacts premature. An unambiguous study of these materials will require greater capacity for material throughput, so a greater variety of fibers and modifications may be probed in far higher number of replicates. Until such time as our scaled spinning operations come online, we are limited to the observation of fracture faces to draw conclusions about the nature of the composite failure.

Figure 8 shows the fracture face of tensile specimens for e-spun mats in epoxy both with and without the PEI additive. The smaller-diameter fiber mats are shown as panels a and b, while the larger mats are represented by c and d. The reference nylon sample exhibits substantial debonding of the fiber from the epoxy matrix, and clear evidence of individual fiber pull-out and deformation is apparent. The fiber mat spun with PEI additive shows improved bonding with the epoxy matrix. The fibers appear broken on the same plane with the matrix and did not exhibit pull-out or debonding. The behavior of the fiber is more easily observed considering 8c and 8d, as the larger fiber diameters facilitate their unambiguous identification. Similar behavior was observed for the

smaller fibers but was more difficult to ascertain (8a and 8b). The unmodified nylon fibers show several areas of bare fiber, while the modified mat shows better integration of the mat with the matrix. These samples indicate that the orientation of the smaller fibers in the composite was more random than the larger fibers, which was not apparent during the imaging of the initial mats. This might suggest some deformation of the smaller fiber mats during composite preparation.

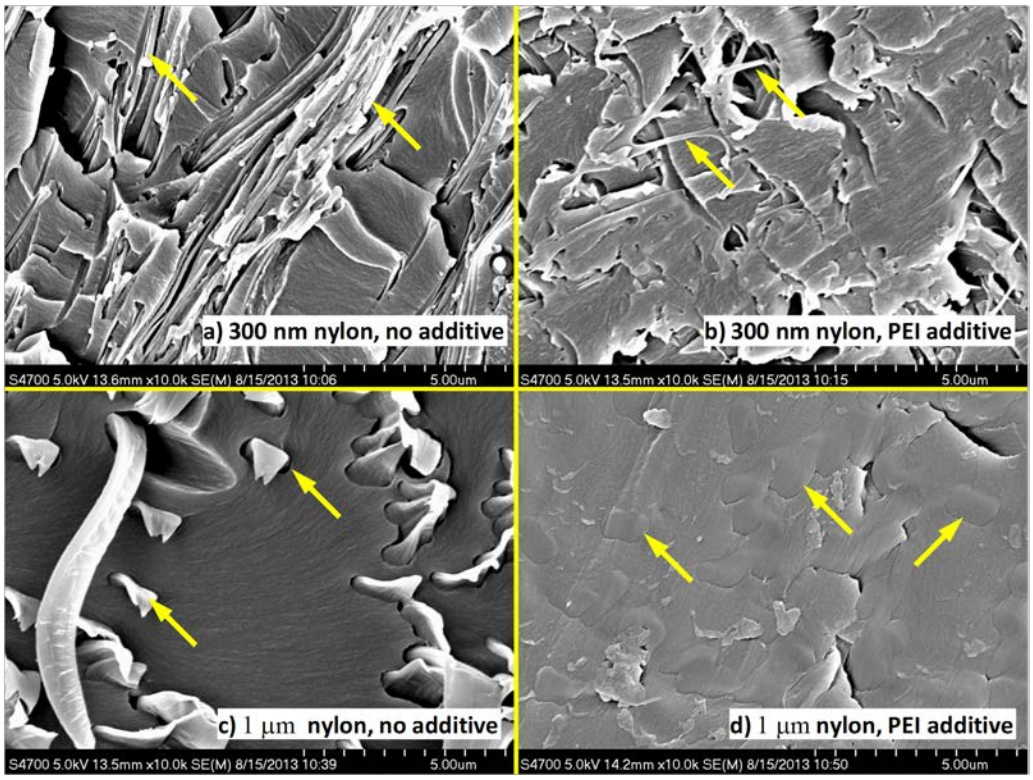

Figure 8. Fracture faces of tensile specimens, arrows point to fiber structures for clarity.

7. Conclusion

A series of oriented e-spun nylon fibers were prepared with nominal fiber diameters of 300 nm and 1 μm. A series of mats were also prepared that contained a hyperbranched PEI to provide for surface modification of the fibers. The mats were used to prepare composites reinforced with the nanofibers, which were interrogated using techniques such as DMA and tensile testing. While the nanofibers did not dramatically stiffen the resulting composites, they provided insight as to the impact of the additives on the interaction of the fibers with the composite matrix. The inclusion of the HBP-PEI appeared to improve interfacial interactions of the fibers with the matrix, as reduced void content and uniform fracture interfaces were observed in the modified composites. No conclusion could be drawn regarding the impact of fiber diameter on fiber modulus, as the specimens studied did not show consistent trends when comparing fibers of

diameter ca. 1 μm and 300 nm. The fiber mats prepared for this study limited the scope and accessibility of test specimens; the results from the examination of fiber-matrix interfaces argue for further investigation. The recent reports of improved composites through nanofiber reinforcement suggest the promise of nanofiber technology, which should be actively revisited as our nanofiber-forming capabilities expand.

8. References

1. Dietzel, J. M.; Kleinmeyer, J. D.; Hirvonen, J. K.; Beck Tan, N. C. Controlled Deposition of Electrospun Poly(Ethylene Oxide) Fibers. *Polymer* **2001**, *42*, 8163–8170.

2. Wang, N.; Wang, X.; Ding, B.; Yu, J.; Sun, G. Tunable Fabrication of Three-Dimensional Polyamide-66 Nano-Fiber/Nets for High Efficiency Fine Particulate Filtration. *J. Mater. Chem.* **2012**, *22*, 1445–1452.

3. Zander, N. E. Hierarchically Structured Electrospun Fibers. *Polymer* **2013**, *5*, 19–44.

4. Pai, C-L.; Boyce, M. C.; Rutledge, G. C. Mechanical Properties of Individual Electrospun PA 6(3)T Fibers and Their Variation with Fiber Diameter. *Polymer* **2011**, *52*, 2295–2301.

5. Papkov, D.; Zou, Y.; Andalib, M. N.; Goponenko, A.; Cheng, S. Z. D.; Dzenis, Y. A. Simultaneously Strong and Tough Ultrafine Continuous Fibers. *ACS Nano.* **2013**, *7*, 3324–3331.

6. Chronakis, I. S. Novel Nanocomposites and Nanoceramics Based on Polymer Nanofibers Using Electrospinning Process – A Review. *J. Mater. Processing Tech.* **2005**, *167*, 283–293.

7. Lin, S.; Cai, Q.; Ji, J.; Sui, G.; Yu, Y.; Yang, X.; Ma, Q.; Wei, Y.; Deng, X. Electrospun Nanofiber Reinforced and Toughened Composites Through In Situ Nano-Interface Formation. *Composites Sci. Tech.* **2008**, *68*, 3322–3329.

8. Liao, H.; Wu, Y.; Wu, M.; Liu, H. Effects of Fiber Surface Chemistry and Roughness on Interfacial Structures of Electrospun Fiber Reinforced Epoxy Composite Films. *Polymer Composites* **2011**, *32*, 837–845.

9. Tian, M.; Gao, Y.; Liu, Y.; Liao, Y.; Xu, R.; Hedin, N.E.; Fong, H. Bis-GMA/TEGDMA Dental Composites Reinforced With Electrospun Nylon 6 Nanocomposite Nanofibers Containing Highly Aligned Fibrillar Silicate Single Crystals. *Polymer* **2007**, *48*, 2720–2728.

10. Bilge, K.; Ozden-Yenigun, E.; Simsek, E.; Menceloglu, Y.Z.; Papila, M. Structural Composites Hybridized With Epoxy Compatible/Polymer/MWCNT Nanofibrous Interlayers. *Comp. Sci. and Technol.* **2012**, *72*, 1639–1645.

11. Magniez, K.; Chaffraix, T.; Fox, B. Toughening of a Carbon-Fibre Composite Using Electrospun Poly(Hydroxyether of Bisphenol A) Nanofibrous Membranes Through Inverse Phase Separation and Inter-Domain Etherification. *Materials* **2011**, *4*, 1967–1984.

12. Hamer, S.; Leibovich, H.; Green, A.; Intrater, R.; Avrahami, R.; Zussman, E.; Siegmann, A.; Sherman, D. Mode I Interlaminar Fracture Toughness of Nylon 66 Nanofibrilmat Interleaved Carbon/Epoxy Laminates. *Polymer Composites* **2011**, *32*, 1781–1789.

13. Chen, Q.; Zhang, L.; Rahman, A.; Zhou, Z.; Wu, X-F.; Fong, H. Hybrid Multi-Scale Epoxy Composite Made of Conventional Carbon Fiber Fabrics With Interlaminar Regions Containing Electrospun Carbon Nanofiber Mats. *Composites: Pt. A.* **2011**, *42*, 2036–2042.

14. Sihn, S.; Kim, R. Y.; Huh, W.; Lee, K-H.; Roy, A.K. Improvement of Damage Resistance in Laminated Composites With Electrospun Nano-Interlayers. *Comp. Sci. Tech*. **2008**, *68*, 673–683.

15. Zhang, J.; Lin, T.; Wang, X. Electrospun Nanofibre Toughened Carbon/Epoxy Composites: Effects of Polyetherketone Cardo (PEK-C) Nanofibre Diameter and Interlayer Thickness. *Comp. Sci. Tech*. **2010**, *70*, 1660–1666.

16. Zhang, J.; Yang, T.; Lin, T.; Wang, C. H. Phase Morphology of Nanofibre Interlayers: Critical Factor for Toughening Carbon/Epoxy Composites. *Comp. Sci. Tech*. **2012**, *72*, 256–262.

17. Yasaee, M.; Bond, I. P.; Trask, R. S.; Greenhalgh, E. S. Mode I Interfacial Toughening Through Discontinuous Interleaves for Damage Suppression and Control. *Composites: Pt. A* **2012**, *43*, 121–128 and 198–207.

18. Malmström, E.; Johansson, M.; Hult, A. Hyperbranched Aliphatic Polyesters. *Macromolecules* **1995**, *28*, 1698–1703.

19. Orlicki, J. A.; Kosik, W. E.; Demaree, J. D.; Bratcher, M. S.; Jensen, R. E.; McKnight, M. S. Surface Segregation of Branched Polyethylenimines in a Thermoplastic Polyurethane. *Polymer* **2007**, *48*, 2818–2826.

20. Ding, B.; Wang, X.; Yu, J.; Wang, M. Polyamide 6 Composite Nano-Fiber/Net Functionalized by Polyethyleneimine on Quartz Crystal Microbalance for Highly Sensitive Formaldehyde Sensors. *J. Mater. Chem*. **2011**, *21*, 12784–12792.

21. Hunley, M. T.; Harber, A.; Orlicki, J. A.; Rawlett, A. M.; Long, T. E. Effect of Hyperbranched Surface-Migrating Additives on the Electrospinning Behavior of Poly(Methyl Methacrylate). *Langmuir* **2008**, *24*, 654–657.

INTENTIONALLY LEFT BLANK.

Appendix. Supplemental Data

Additional synthetic targets were identified, as it was intended to create hyperbranched polymer (HBP)-based additives with a hybrid linear-dendritic structure. These materials were intended to be formed separately and then combined using highly efficient "click" chemistry. This is a term that refers to highly thermodynamically favored reactions that proceed with rapid kinetics, good regio- and stereo specificity, and low occurrence of side reactions.[1] The classic "click" reaction is the Huisgen's 1,2-dipolar cycloaddition between an alkyl azide and a terminal alkyne to yield a triazine linker. To that end, both HBP and linear polymer analogs were prepared that would possess clickable functional groups, as shown in figures A-1 and A-2.

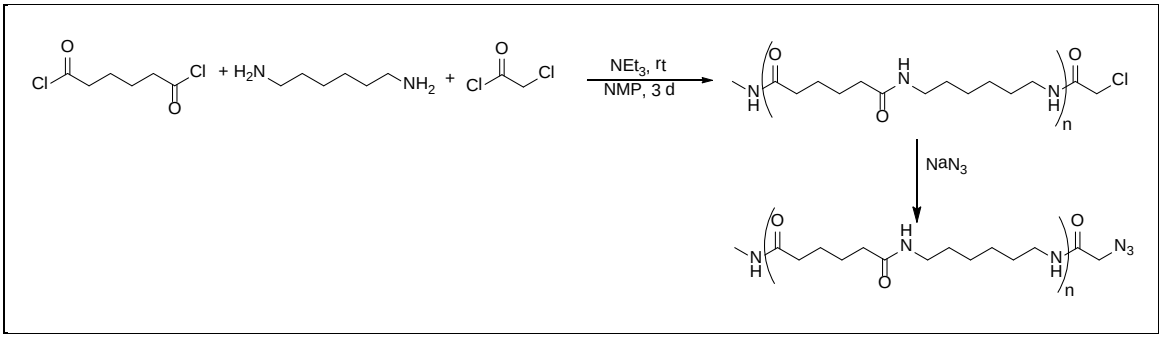

Figure A-1. Preparation of azide-terminated nylon oligomer.

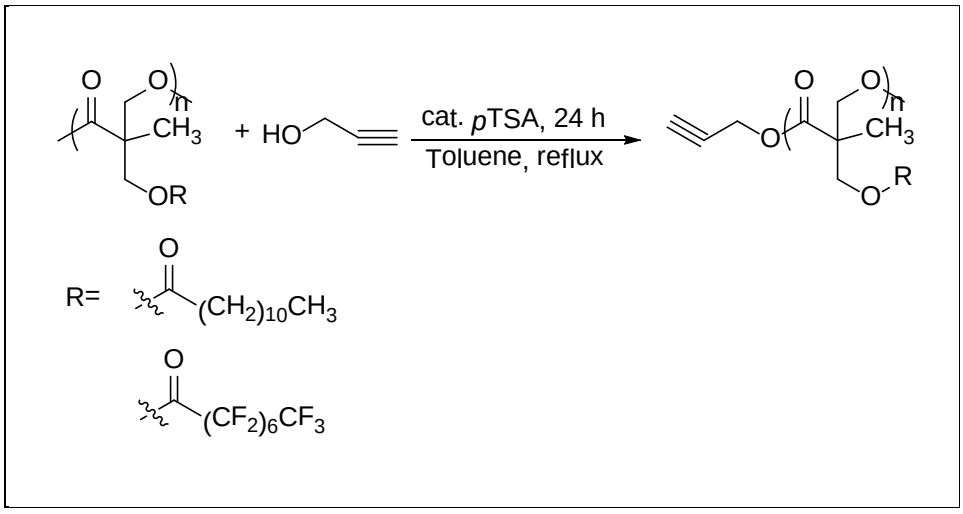

Figure A-2. Preparation of modified PE with alkyne focal point.

The nylon-azide oligomer shown in figure A-1 would first result in a potentially complex mixture of nonfunctional chains along with mono- and di-terminated alkyl halides. The product distribution was governed by the $A_2 + B_2$ nature of the classic nylon polymerization and is a function of amine terminal groups available on the polymer when the 2-chloroacetyl chloride

[1] Iha, R. K.; Wooley, K. L.; Nystrom, A. M.; Burke, D. J.; Kade, M. J.; Hawker, C. J. Applications of Orthogonal "Click" Chemistries in the Synthesis of Functional Soft Materials. *Chem. Rev.* **2009**, *109*, 5620–5686.

was added to the reaction mixture. The preparation of PE modified with an alkyne focal point faced similar issues, as commercial Boltorn H20 typically possesses a tetra-functional core from which the HBP material is grown radially. The reaction conditions were sufficient to permit insertion of the alkyne at the focal point of a pseudo-Dendron wedge through trans-esterification. Both product mixtures were therefore complex and were not purified further. The issues we experienced when using the PE-MAc additive meant that the realization of the desired dumbbell or tadpole architecture would likely be very difficult to characterize and exhibit poor solubility/stability. As a result, the products of figures A-1 and A-2 were initially pursued but were ultimately abandoned with minimal analysis of the final products.

Stress/strain curves are shown in figures A-3 through A-6 for composite samples on a common axis.

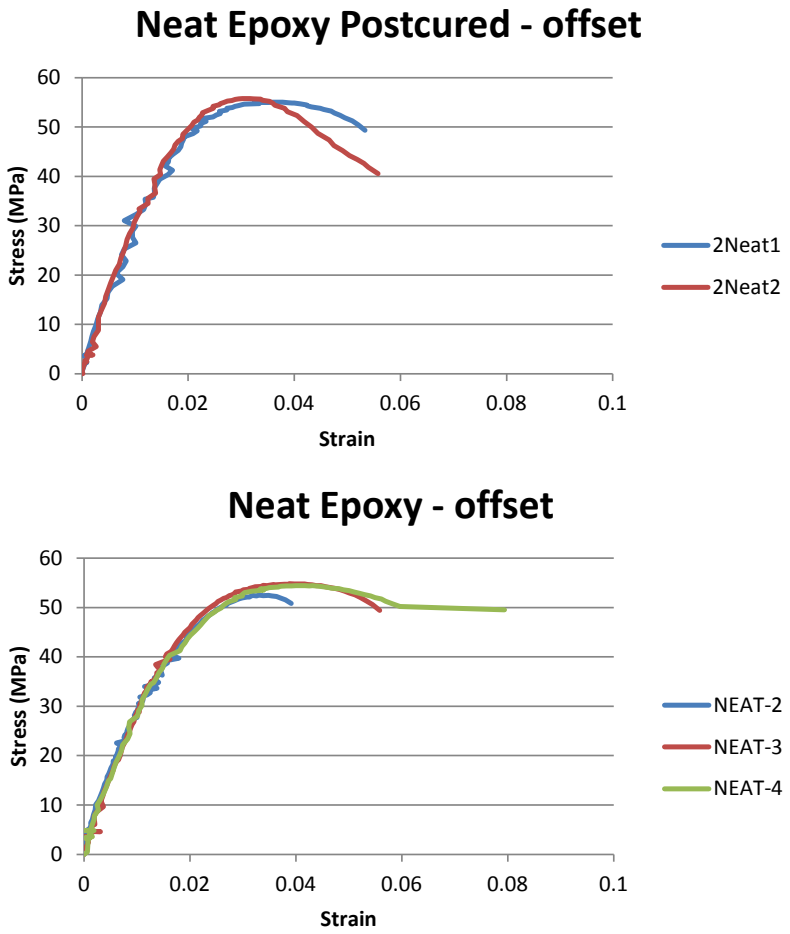

Figure A-3. Tensile data for neat epoxy samples, both with and without a postcure.

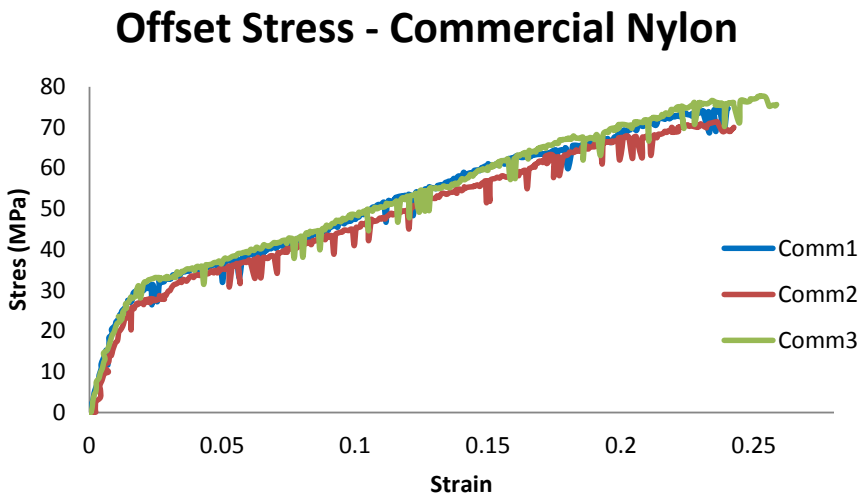

Figure A-4. Tensile data for epoxy specimens reinforced with commercial nylon fabric.*

* Commercial fibers were obtained in nylon fabric, which included a mat with a 0°/90° weave, likely resulting in the abnormally large elongation observed in the figure (i.e., deformation of the fiber weave resulted in the large strain).

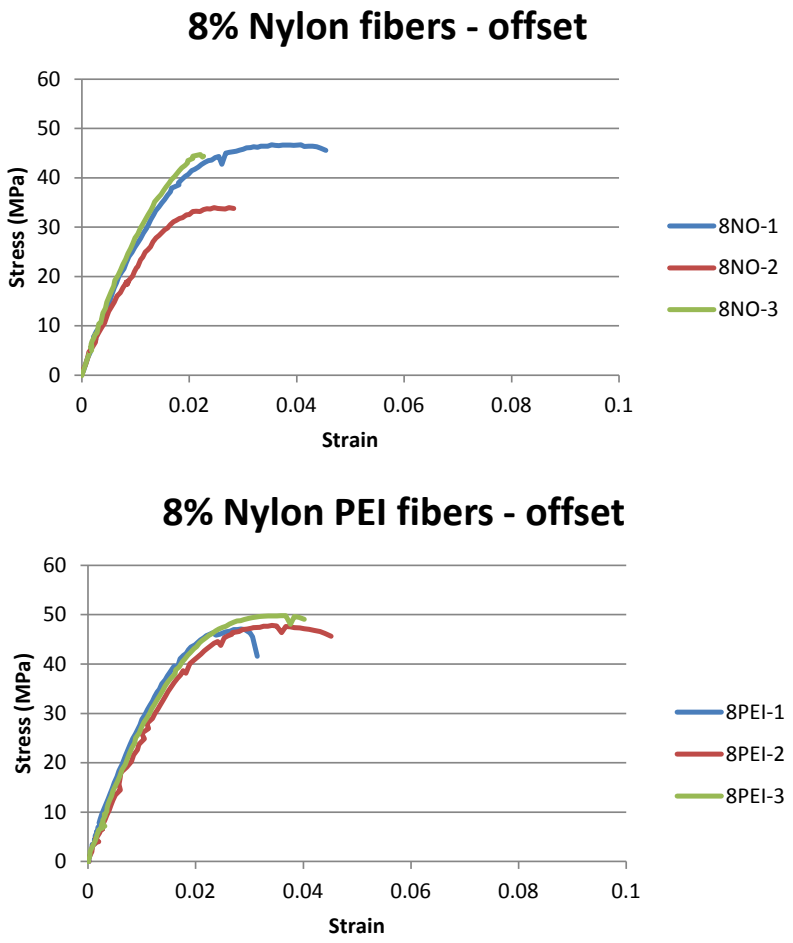

Figure A-5. Tensile data for epoxy specimens reinforced with e-spun nylon fabric of ca. 1-μm diameter. Top curves contained nylon mats containing 2% PEI HBP modifier, and bottom curves represent samples containing the as-spun nylon.

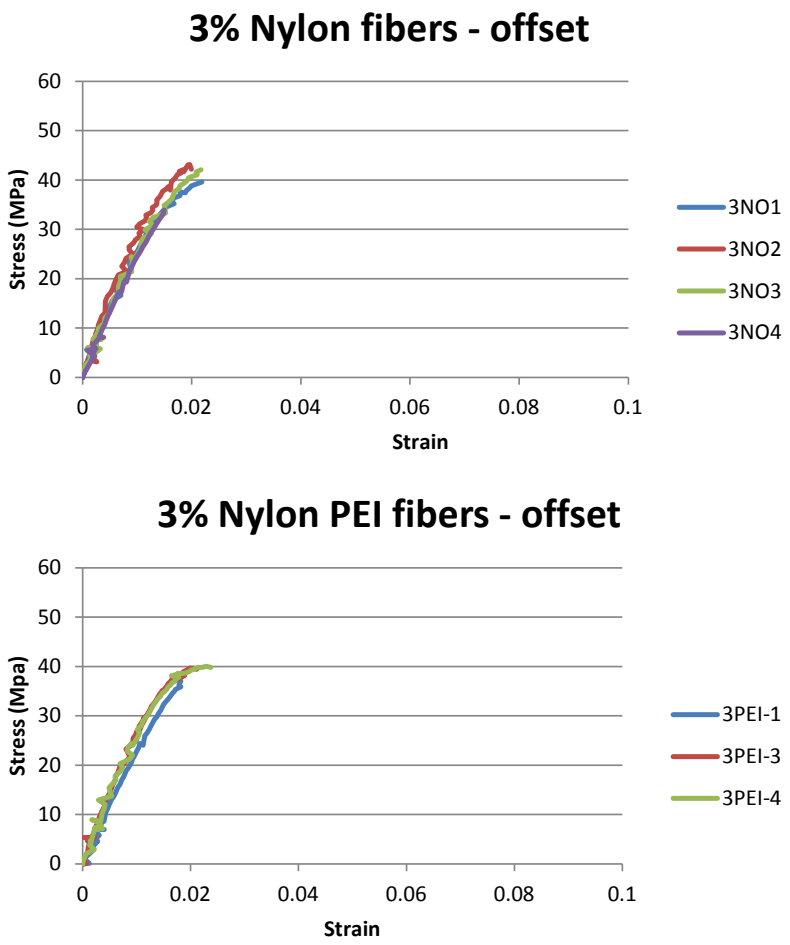

Figure A-6. Tensile data for epoxy specimens reinforced with e-spun nylon fabric of ca. 300-nm diameter. Bottom curves contained nylon mats containing 2% PEI HBP modifier, top curves represent samples containing the as-spun nylon.

NO. OF COPIES	ORGANIZATION
1 (PDF)	DEFENSE TECHNICAL INFORMATION CTR DTIC OCA
1 (PDF)	DIRECTOR US ARMY RESEARCH LAB IMAL HRA
1 (PDF)	DIRECTOR US ARMY RESEARCH LAB RDRL CIO LL
1 (PDF)	GOVT PRINTG OFC A MALHOTRA
1 (PDF)	DIR USARL RDRL WMM G J A ORLICKI

INTENTIONALLY LEFT BLANK.